

# Effects of Knock Intensity Measurement Technique and Fuel Chemical Composition on the Research Octane Number (RON) of FACE Gasolines: Part 2 – Effects of Spark Timing

Alexander Hoth, Christopher P. Kolodziej

Argonne National Laboratory, 9700 S. Cass Avenue, Lemont, IL 60439, USA

**Keywords:** RON, Knock-limited spark advance, Lambda effects, Knock characterization

## 10 Abstract

11 The Research and Motor Octane Number (RON, MON) characterize a fuel's knock resistance by rating  
12 the knock intensity of a sample fuel relative to that of Primary Reference Fuels (PRF) in a Cooperative  
13 Fuel Research (CFR) Engine. A fuel's octane number is regulated to prevent damage from autoignition  
14 leading to knocking combustion in spark-ignition engines. The operational differences between the  
15 standard RON rating and modern engine operation are explored in a three-part publication series. The  
16 previous study focused on the effects of lambda and knock characterization. This second study primarily  
17 focuses on the effects of spark timing on RON determination. Following the findings from the first  
18 publication, the knock intensity was captured by the knockmeter and by the maximum amplitude of  
19 pressure oscillations (MAPO) at the lambda of peak knock intensity and stoichiometry. Knock-limited  
20 spark advance tests were conducted for a set of seven Fuels for Advanced Combustion Engines (FACE)

21 from the Coordinating Research Council (CRC) with varying chemical composition, PRFs, and Toluene  
22 Standardization Fuels (TSFs). For retarded spark timings, pre-spark low-temperature heat release was  
23 found for low RON PRFs. Low RON PRFs also showed knocking characteristics before reaching the center  
24 of combustion suggesting that the use of knock-limited spark advance (KLSA) was preferred over the  
25 knock-limited combustion phasing. Primarily paraffinic fuels tended towards increased pressure  
26 oscillations while dominantly aromatic fuels experienced higher pressure rise rates. A MAPO-based KLSA  
27 correlated best to Octane Index at a negative K-factor suggesting beyond RON operation despite being  
28 at otherwise RON conditions. At stoichiometry, the MAPO-based KLSA did neither correlate to RON nor  
29 Octane Index. Good agreement was found between KLSA-based effective RON from this study to the  
30 MAPO-based effective RON from the first study.

31    **1. Introduction**

32

33    Modern engines push towards higher engine efficiency through means of an increased compression  
34    ratio and downsizing in combination with boosting. Those technologies increase pressure and  
35    temperature in the combustion chamber of spark-ignition engines, which can lead to an undesired  
36    cascading autoignition and subsequently potentially harmful high-frequency pressure oscillations called  
37    knock [1]. The research (RON) and motor octane number (MON) are fuel properties that characterize  
38    the fuel's resistance to autoignition [2, 3]. However, the assessment of RON and MON compared to the  
39    knock-limited operation of modern commercial engines differ significantly as outlined in *Table 1*.

40    RON and MON rate the knock intensity of a sample fuel relative to the knock intensity of two bracketing  
41    primary reference fuels (PRF) [2]. However, the knock intensity is assessed with a knockmeter system  
42    which attenuates high-frequency pressure oscillations as outlined by multiple studies [4 - 7]. On the  
43    other hand, modern research engines limit the maximum amplitude of pressure oscillations (MAPO)  
44    during operation [4, 6, 8, 9]. Concern exists about using MAPO as a metric to indicate knock because  
45    pressure oscillations are in-cylinder acoustics which may or may not be related to autoignition in all  
46    cases. For example, combustion of fast burning fuels such as hydrogen may produce pressure  
47    oscillations even when there is no autoignition. However, the gasolines used for this study have a more  
48    conventional (slower) heat release rate which does not typically induce any pressure oscillations. For  
49    this study, MAPO is calculated as the peak value of a band-pass filtered (4 – 18 kHz) and rectified  
50    cylinder pressure signal. More details about the calculation of MAPO can be found in the previous  
51    publication [4]

52    The octane numbers of the fuels are assessed at the lambda of the highest knock intensity which equals  
53    the worst performance of the fuel. The first study of this three-part publication series and a previous  
54    study by the authors found the lambda of peak knock intensity, both knockmeter- and MAPO-based, to

55 occur at fuel-rich conditions. Ethanol as well as olefins and cycloparaffins shifted the lambda of peak  
56 knock closer toward stoichiometry [4, 10, 11]. The value of lambda at peak MAPO and peak knockmeter  
57 occurs typically within close proximity of each other [4, 12].

58 The octane numbers are rated on the Cooperative Fuel Research (CFR) engine which has a variable  
59 compression ratio adjustable to the respective octane number of the sample fuel while in operation.  
60 Modern research engines typically have a fixed, but interchangeable compression ratio. Due to the fixed  
61 compression ratio, modern engines have to retard the spark timing to limit knocking combustion at high  
62 load operating conditions. The knock-limited combustion phasing (KLCA50) and the knock-limited spark  
63 advance (KLSA) are typical ways to identify the knock limit of a modern research engine at a given  
64 pressure-based MAPO knock intensity threshold [9, 13]. During RON rating, the CFR engine has a fixed  
65 spark timing at 13°bTDC (-13°aTDC) and rates the variable knockmeter-based knock intensity [2]. This is  
66 opposing the variable spark timing operation for maintaining a fixed MAPO-based knock intensity  
67 threshold in modern SI engines.

68 *Table 1. Overview of the discrepancy in operating conditions between the RON rating procedure and knock-limited spark  
69 advance type testing utilized in modern commercial engines.*

Parameter	RON Rating [2]	KLSA type testing
<b>Knock Intensity</b>	CFR knockmeter system	Cylinder pressure oscillations
<b>Lambda</b>	Peak knockmeter reading	Generally stoichiometric
<b>Spark Timing</b>	Constant at 13°bTDC (-13°aTDC)	Limited by incipient knock
<b>Compression Ratio</b>	Variable, depending on RON	Fixed / Interchangeable

70  
71 The differences in the rating methodology between the RON assessment and modern engine operation  
72 lead to discrepancies between the RON of a gasoline and its actual knock limiting quality in modern

73 engines [6, 8, 12, 13]. Other operating conditions, such as the slow CFR engine speed of 600 rpm and the  
74 side-mounted spark plug in the CFR engine can contribute to the reported discrepancy as well. Yates et  
75 al. showed the pressure-temperature trajectories of standard RON and MON tests and the impact of  
76 modern engine technologies such as direct injection and turbocharging. This shifted the pressure-  
77 temperature trajectory towards higher pressures into the beyond RON region [14]. Kalghatgi proposed  
78 the Octane Index (OI) which uses an engine operation-specific weighting factor K to interpolate or  
79 extrapolate between the RON and MON trajectory, equation 1. The RON trajectory represents a K-factor  
80 of K = 0 while MON is represented when K = 1 [15, 16]. Mittal et al. showed, that historically, in the  
81 1950s, K-factors between 0 and 1 were representative of engine performance. Modern engine operation  
82 as of 2009 resulted in a range of K = -0.6 to 0.2 [17]. A negative K-factor leads to a higher Octane Index  
83 with increased RON-MON sensitivity and therefore higher knock resistance for lower MON values for a  
84 fuel with a given RON [13, 17].

85 
$$OI = RON - K * (RON - MON) \quad (\text{Equ. 1}) [15]$$

86 The combustion phasing plays a critical role in engine efficiency and knock prevention. The RON test  
87 utilizes a constant spark timing which leads to a variation of the center of combustion solely due to  
88 differences in the laminar flame speed of the fuel. The center of combustion is identified as the crank  
89 angle of 50% mass fraction burned (CA50). Ethanol was previously found to slightly advance the  
90 combustion phasing during flame propagation [10, 18].

91 Hauber et al. proposed a novel gasoline knock index, which utilized a variable spark timing to maintain a  
92 constant CA50 [11]. Other updates include rating the knock intensity of fuels based on pressure  
93 oscillations and operating the CFR engine at stoichiometry [11]. The rating methodology showed good  
94 agreement between the gasoline knock index and RON but did not address the discrepancy between  
95 RON and knock limited combustion phasings in modern engines.

96 Multiple studies from Syzbist et al, Pulpeiro Gonzalez et al., and Vuilleumier et al. showed KLSA type  
97 testing for the Co-Optima core fuels in SI modern engines [13, 19, 20]. These fuels are blended to a  
98 constant RON of 98 while changing the chemical composition from highly paraffinic to highly aromatic  
99 and also include a RON 98 fuel with 30 vol% ethanol. While at a constant RON of 98, those fuels  
100 significantly varied in their KLCA50 as summarized in a previous study by the authors [12].

101 Low-temperature heat release is typically seen during homogenous charge compression ignition but a  
102 recent study by the authors found that low-temperature chemistry also occurs during spark ignition  
103 combustion while being covered up by the main heat release from the propagating flame [21].  
104 A significant retard in spark timing could visualize such pre-spark low-temperature chemistry.

105 The first part of this three-part publication series explored the effects of switching from a knockmeter-  
106 based knock intensity assessment to a MAPO-based knock threshold as well as switching from the  
107 lambda of peak knock intensity to stoichiometry (rows one and two from *Table 1*). The knockmeter  
108 system was found to filter out high-frequency signal components typically associated with knocking  
109 combustion. Despite the differences in knock measurement principle, the lambda of peak knockmeter  
110 and lambda of peak MAPO closely matched. Based on a MAPO knock threshold of 0.1 bar, all cycles for  
111 the CRC fuels were knocking during standard RON testing. Significant offsets between the standard RON  
112 rating and the MAPO-knock intensities at standard RON operation were found. The best correlation  
113 between the MAPO knock intensity under standard RON conditions and Octane Index was found for  $K =$   
114  $-0.48$  which would represent standard RON operation but using a MAPO-based knock intensity [4].

115 This study rated the seven CRC FACE fuels via a knock-limited spark advance (KLSA) test similar to  
116 modern engine knock characterization (row three of *Table 1*). The tests were performed at  
117 stoichiometry as well as at the lambda of the highest knock intensity following the findings from the first  
118 paper. Both the knockmeter-based and the MAPO-based knock intensity of the sample fuels were rated

119 relative to PRFs to calculate an equivalent RON based on the fuel's KLSA. A comparison to the standard  
120 RON ratings of the fuels showed vastly different levels of correlation to standard RON depending on the  
121 type of knock intensity measurement technique as well as the applicable lambda. Further, a comparison  
122 to the effective MAPO-based RON calculations from the first paper was explored.

123

124 **2. Experimental Procedures**

125

126 For this experimental study, a single-cylinder, variable compression ratio, naturally aspirated, and  
127 carbureted CFR F1 engine was used. This represents the standard octane rating engine for RON  
128 conditions according to ASTM D2699. The engine was upgraded to encompass modern research engine  
129 measurement equipment, such as an indicated cylinder pressure measurement via a measuring spark  
130 plug and a wide-band lambda sensor. In addition, the spark timing was monitored using a current clamp.  
131 More details about the used sensors and a full list of installed measurement devices are included in  
132 *Table 5* in the appendix and listed in the first part of this publication series [4]. It is important to note,  
133 that no changes to the geometry of intake, cylinder, or exhaust were made to retain the engine  
134 compliance with the ASTM D2699 method [2].

135 Seven fuels for advanced combustion engines (FACE) from the Coordinating Research Council (CRC)  
136 were tested in this study. *Table 2* summarizes the octane numbers, the 90% evaporation temperature,  
137 and the composition of each FACE gasoline. Based on their composition, the FACE fuels were  
138 characterized as mainly paraffinic or mainly aromatic fuels. Each of the two groups also includes  
139 gasolines that have olefins, cycloparaffins or 15 vol% ethanol added. Additional details are included in  
140 previous CRC reports and the first part of this publication series [4, 22]. Both this study and the previous

141 study compare the seven FACE fuels to numerous bracketing PRFs and two applicable toluene  
142 standardization fuels (TSFs) as specified in the ASTM D2699 method.

143

144 *Table 2. Fuel overview with physical properties and chemical composition.*

145 *O – Olefin, cP – Cyclo-Paraffinic, E15 – 15 vol Ethanol [22]*

FACE Fuel	RON	MON	S	T90 (°F)	Iso-paraffin (vol%)	Aromatic (vol%)	N-Paraffin (vol%)	Cyclo-Paraffin (vol%)	Olefin (vol%)	Categorization	Symbol
B	95.8	92.4	3.4	236	86.9	5.8	8.0	0.1	0.02	Iso-paraffinic	■
D	94.2	87.0	7.2	331	42.1	33.4	24.1	0.1	0.04	Aromatic	■
F	94.0	88.1	5.9	242	67.6	7.7	4.4	11.0	9.4	Iso-paraffinic, O, cP	▲
G	96.5	85.8	10.7	343	38.4	33.6	6.7	11.5	8.1	Aromatic, O, cP	▲
A + E15	94.8	89.4	5.4	219	73.1	0.3	9.9	1.4	0.2	Iso-paraffinic, E15	□
C + E15	94.8	88.8	6.0	241	59.3	3.3	20.8	0.3	1.1	Iso-paraffinic, E15	□
H + E15	94.1	83.3	10.8	323	19.4	30.4	19.1	8.9	5.8	Aromatic, O, cP, E15	△

146

147 Key differences between standard RON testing and modern engine knock rating were summarized in

148 *Table 1.* For this testing, variations of the standard RON test were established to mimic the knock rating

149 procedure of modern engines by varying the spark timing to achieve pre-defined knock intensity

150 thresholds. The knockmeter knock intensity was limited to 40 knock units (KU) while the MAPO

151 threshold was set to 0.6 bar for a cyclic average across 300 consecutive cycles. The 0.6 bar MAPO

152 threshold represents a 1 bar/1000 rpm knock threshold at the RON engine speed of 600 rpm, which is a

153 commonly used knock intensity threshold for modern engine knock calibration. *Figure 1* shows a spark

154 timing sweep for iso-octane (PRF100) at otherwise standard RON conditions. At the standard spark

155 timing of 13 degrees before top dead center (-13°aTDC), the MAPO knock intensity is significantly higher

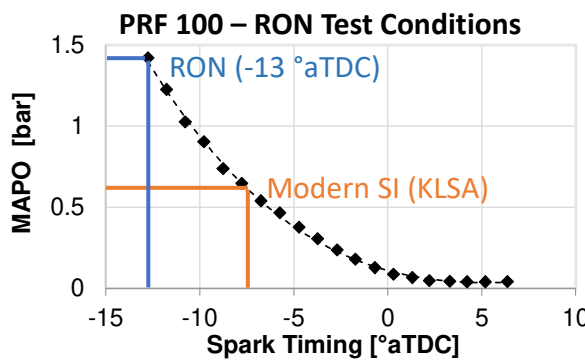
156 than the defined knock intensity threshold. When retarding the spark timing, the knock intensity

157 dropped due to less intense pressure-temperature conditions in the cylinder. The spark timing at which

158 the knock intensity threshold is reached is termed knock-limited spark advance (KLSA). When plotted

159 versus the center of combustion, this is termed knock-limited crank angle of 50 % mass fraction burned

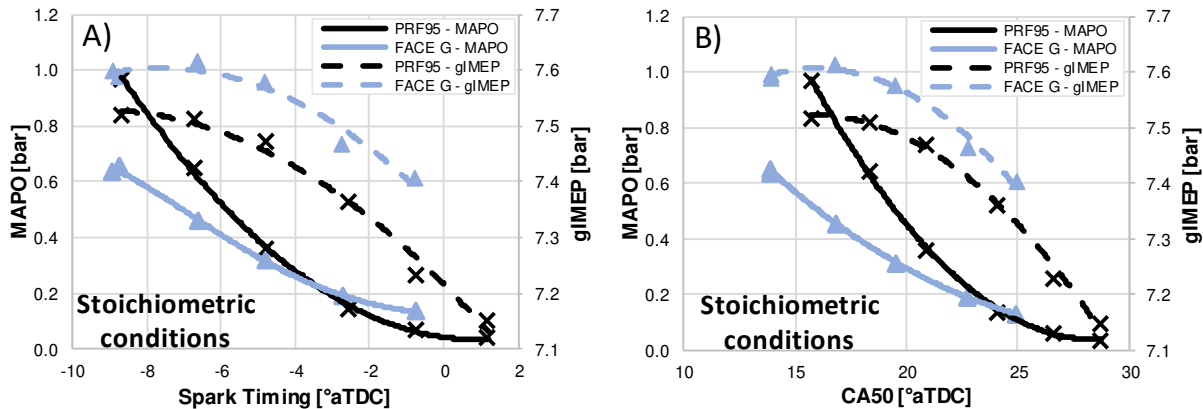
160 (KLCA50). The mass fraction burned was calculated using the Thermodynamics 2 function of AVL  
161 Concerto. This function calculates the apparent heat release with gamma dependent on an estimated  
162 charge temperature.



163

164 *Figure 1. Pressure-based MAPO knock intensity of the standard RON test and its knock-limited spark advance (KLSA) limits*

165 The first set of testing was performed under RON-like conditions at the lambda of highest knock  
166 intensity at the standard compression ratio for a RON 95 sample as defined by the ASTM D2699 method.  
167 Following the findings from the previous study, the second set of testing was performed at  
168 stoichiometry to better represent modern engine operation. Testing performed at stoichiometry  
169 reduced both the knockmeter and the pressure-based knock intensities [4]. To increase the knock  
170 intensities when testing at stoichiometry, an increased compression ratio was selected. Using an  
171 iterative procedure, the compression ratio and center of combustion (CA50) were varied to reach the  
172 0.6 bar MAPO threshold and the combustion phasing of maximum gross indicated mean effective  
173 pressure (gIMEP) for FACE-G,  
174 *Figure 2. This compression ratio was maintained for all other sample and reference fuels. FACE-G was*  
175 *selected since it showed the overall lowest MAPO knock intensities in the previous study [4]. Therefore,*  
176 *all other FACE fuels should require a retarded spark timing relative to FACE-G to limit the knock*  
177 *intensity.*



178

179 *Figure 2. MAPO and the gross indicated mean effective pressure (gIMEP) as a function of spark timing and CA50.*

180 *Figure 2 shows the performed initial spark timing sweeps and the MAPO knock intensity as well as gross*  
 181 *indicated mean effective pressure response for FACE-G and PRF95. Figure 2A shows the variation of the*  
 182 *spark timing while Figure 2B has the same information depicted based on the center of combustion*  
 183 *(CA50). The CA50 represents the crank angle location of 50 percent mass fraction burned. Figure 2A and*  
 184 *Figure 2B show very similar trends of increasing knock intensities for advanced combustion phasing*  
 185 *while gIMEP follows a parabolic shape. FACE-G has a higher gIMEP compared to PRF95. This is due to a*  
 186 *slight advance in combustion phasing for FACE-G over PRF95 for a given spark timing. For both fuels, the*  
 187 *maximum gIMEP occurred at a CA50 between 16 and 18 °aTDC. This is significantly later than values*  
 188 *reported for modern engines which typically have their peak gIMEP around 8°aTDC [24]. Part of the*  
 189 *reason is the slow engine speed of 600 rpm and the knocking combustion which constitute to increased*  
 190 *heat transfer losses. The MAPO knock intensity of PRF95 is higher compared to MAPO of FACE-G despite*  
 191 *a higher RON of FACE-G as found in the previous publication and listed in Table 2 [4].*

192 *As mentioned earlier, the compression ratio was set for FACE-G so that a MAPO knock intensity*  
 193 *threshold of 0.6 bar was reached at maximum gIMEP conditions during naturally aspirated operation.*  
 194 *The knock threshold was reached at a spark timing around -9°aTDC (CA50 of 14°aTDC). A slightly more*  
 195 *retarded spark timing resulted in a slight increase in gIMEP, but this is of no further impact as all fuels*

196 were tested at this particular compression ratio and the variation in gIMEP is well within the  
197 measurement uncertainty of 1.5% for the indicated spark plug [25].

198

199 **3. Spark Timing Sweeps**

200

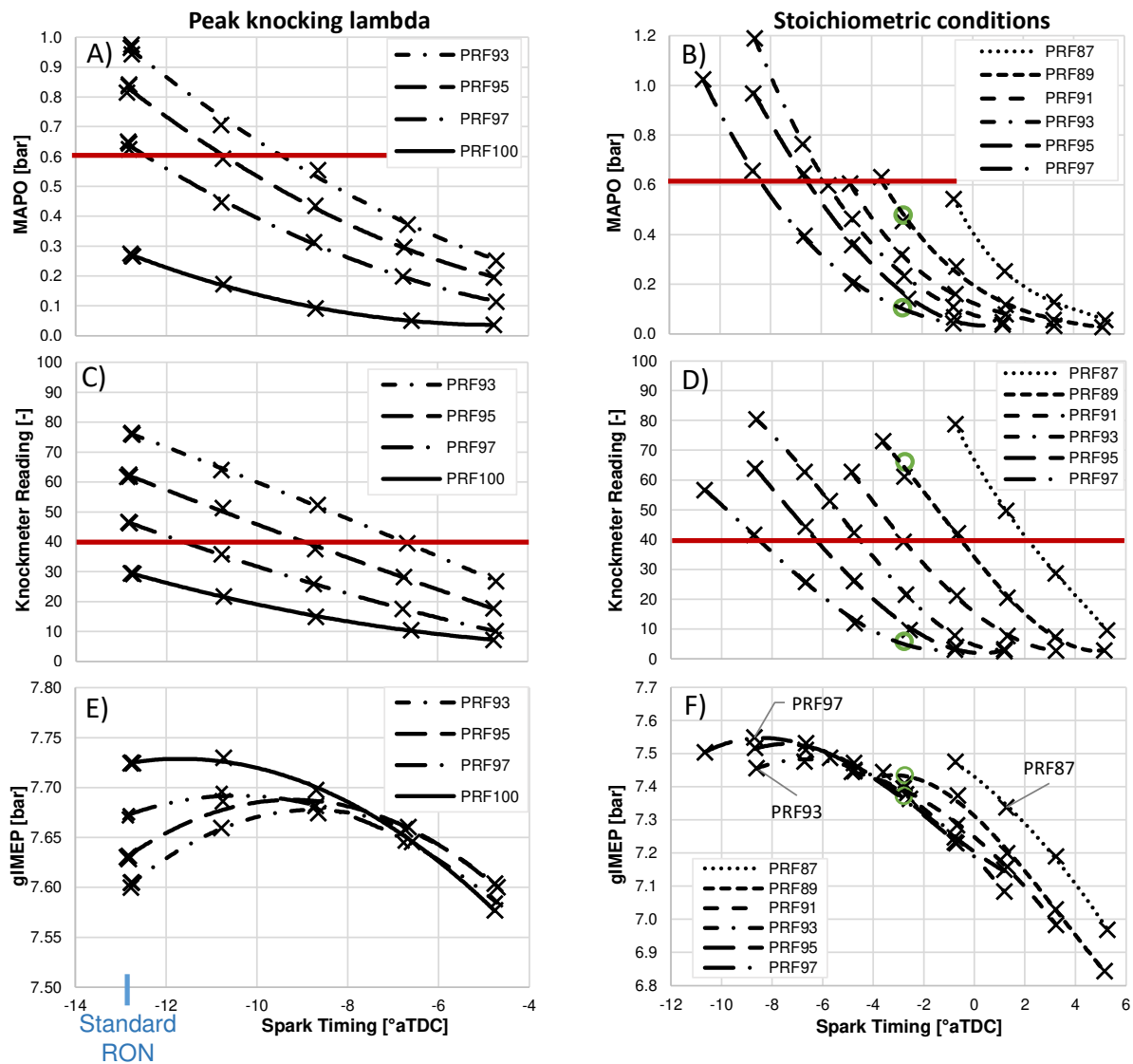
201 **3.1. Primary Reference Fuels**

202 Spark timing sweeps were performed for each fuel at two lambda settings. First, at the lambda of  
203 highest knock intensity, termed peak knocking lambda, and second, at stoichiometry. At standard RON  
204 conditions, meaning peak knocking lambda, the spark timing is defined to -13°aTDC. From this starting  
205 point, the spark timing for PRFs with various RON levels was retarded until the maximum gIMEP was  
206 surpassed. As mentioned earlier, a higher compression ratio was selected for stoichiometric operation,  
207 which resulted in more retarded spark timings compared to peak knocking lambda operation. If tested  
208 at a constant compression ratio, PRFs would have an advanced spark timing for stoichiometric operation  
209 compared to operation at peak knocking lambda. The MAPO and knockmeter knock intensity response,  
210 as well as gIMEP dependence on spark timing, are presented in *Figure 3*. The previous study found  
211 significant differences in fuel performance between operation at the peak knocking lambda and  
212 stoichiometry. Therefore, left-sided plots 3A, 3C, and 3E show conditions for each fuel at its individual  
213 peak knock lambda (PKL) while right-sided plots 3B, 3D, and 3F contain experimental data at  
214 stoichiometry.

215 Advanced spark timings increased both the knockmeter and the MAPO knock intensities. A higher RON  
216 level resulted in lower knock intensities. Because of its high RON relative to the set compression ratio,  
217 PRF100 neither reached the knock threshold of 40 KU nor the threshold of 0.6 bar MAPO for operation

218 at PKL. All other PRFs reached the knock intensity threshold and therefore all cycles of those fuels were  
219 knocking when taking into account the 0.1 bar MAPO threshold from the previous publication [4]. The  
220 PRFs were reasonably linearly spaced and third-order polynomial trendlines were successfully fitted to  
221 the measurement. While not shown in the plot, each trendline had an excellent coefficient of  
222 determination ( $R^2 > 0.99$ ). Therefore, the equation of the trendline can be used to estimate the spark  
223 timing at which the respective PRF crosses either of the knock intensity thresholds of 40 KU or 0.6 bar  
224 MAPO.

225 The gIMEP typically followed a parabolic shape as spark timing was modified. For PKL operation, higher  
226 RON PRFs achieved higher gIMEPs due to lower knock intensities at a given spark timing compared to  
227 lower RON PRFs. It is assumed that increased pressure oscillations penetrate the boundary layer of the  
228 combustion chamber, hence increasing the heat transfer and reducing gIMEP respectively. The PRF100  
229 with the highest RON and therefore lowest knock intensities had the most advanced spark timing for the  
230 maximum gIMEP. At lower knock intensities at retarded spark timings, the gIMEP difference between  
231 PRFs was minimal when operated at PKL conditions. For the stoichiometric cases, a wider range of spark  
232 timings was required to account for the wider range of PRF octane levels. For spark timings after top  
233 dead center, the distribution of gIMEP was more diverse. For example, PRF87 showed an increased  
234 gIMEP at retarded spark timings compared to higher RON PRFs. This is the result of an advanced CA50  
235 for a given spark timing as will be discussed for *Figure 4* and *Figure 5* by analyzing the two green-circled  
236 data points in *Figure 3*.

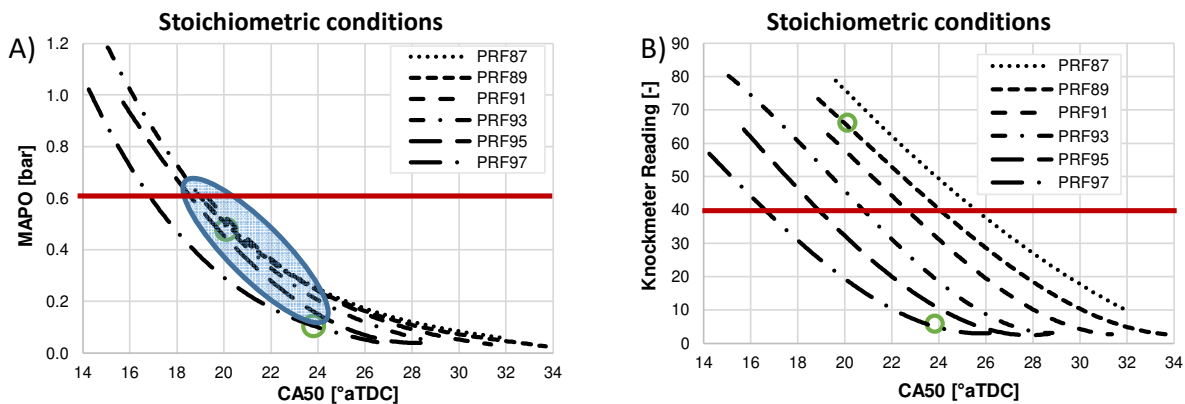


237

238 *Figure 3. Spark timing sweeps at both peak knocking lambda conditions (A, C, E) and stoichiometric conditions (B, D, F) for*  
 239 *MAPO knock intensity, knockmeter knock intensity, and gIMEP for various PRFs. The knock intensity plots show the applied*  
 240 *knock threshold. At stoichiometric conditions, the two green-circled data points are used in Figure 5.*

241 A common way of analyzing spark timing sweeps is to study combustion phasing (CA50). *Figure 4A* and  
 242 *4B* show the MAPO and knockmeter knock intensity response versus CA50. Essentially, *Figure 3B* and  
 243 *Figure 4A* depict identical measurements on a different x-axis. Plots are data point limited to depict the  
 244 trendlines since an excellent correlation ( $R^2 > 0.99$ ) between the trendline and data points was

245 previously shown.  
 246 A cluster of PRFs (circled in blue) is shown in *Figure 4A*. At a given CA50 location (i.e. 20°aTDC), the  
 247 difference of six research octane numbers between PRF87 and PRF93 caused no significant difference in  
 248 the pressure-based knock intensity. This was not expected as a lower RON fuel typically showed higher  
 249 knock intensities as can be seen for the knockmeter knock intensity in *Figure 4B*. The cluster of PRFs was  
 250 not observed when plotting the MAPO on a spark timing basis (*Figure 3B*). The green circled data points  
 251 for PRF97 and PRF89 were captured with a spark timing of -3°aTDC (compare *Figure 3B*) but differ in  
 252 their CA50 location. Therefore, the change in CA50 location is not linearly correlated to changes in spark  
 253 timing. This leads to a close grouping of knock-limited CA50 (KLCA50) for PRFs at the knock threshold of  
 254 0.6 bar MAPO. The knockmeter knock intensity in *Figure 4B* showed less sensitivity towards changes in  
 255 the flame propagation. It is noted, that the described phenomenon was only seen under stoichiometric  
 256 operation, which utilized an increased compression ratio over the standard PKL operation.

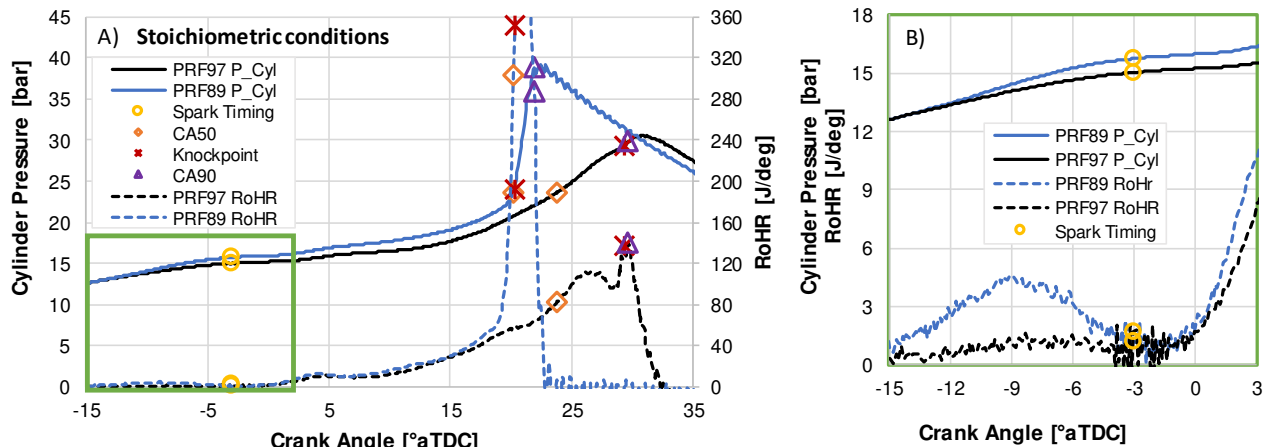


257  
 258 *Figure 4. Knock intensity comparison for PRFs on a CA50 basis at stoichiometric conditions with a cluster of points (blue circled).*  
 259 *The applied knock thresholds are marked as red lines.*  
 260 As previously outlined, the duration between spark timing and the center of combustion (CA50) changes  
 261 with the fuel. *Figure 5* shows a crank-angle resolved cylinder pressure trace and the respective rate of  
 262 heat release for PRF97 (black curve) and a PRF89 (blue curve) at stoichiometric conditions. Both fuels

263 were operated at identical spark timings and were highlighted with green circles in *Figure 3* and *Figure*  
264 4.

265 The representative cycle was selected based on numerous characteristics such as pressure and location  
266 of CA50 and knockpoint, the MAPO knock intensity, the gIMEP, the maximum pressure rise rate and its  
267 location, and the cylinder pressure at spark timing [23]. Therefore, it was ensured to select a pressure  
268 trace that is most representative of each case without using an averaged trace that would average out  
269 knocking characteristics.

270 *Figure 5A* shows the full combustion event from spark timing to end of combustion as characterized by  
271 CA90. The locations of spark timing, CA50, CA90, and knockpoint are marked on the rate of heat release  
272 and on the pressure traces. The PRF89 generally showed a higher pressure trace compared to PRF97  
273 because PRF89 had advanced combustion phasing despite being operated with an identical spark timing.  
274 The CA50 of PRF89 occurs about 3.5 CAD earlier compared to PRF97. Multiple studies discussed the  
275 knockpoint as a typical inflection point in the pressure trace due to cascading autoignition [1, 4, 8, 19].  
276 For PRF89, the crank angle location of knockpoint was almost identical to CA50, which means that  
277 almost 50% of the charge mass auto-ignited. This led to a steep increase in the apparent heat release  
278 and a much-reduced duration from CA50 to CA90 for PRF89. The PRF97 showed slower combustion with  
279 a more delayed center of combustion and knockpoint towards the end of the combustion event. This led  
280 to a lower knock intensity compared to the PRF89 which clearly showed pressure oscillations.



281

282 *Figure 5. Crank angle resolved pressure trace and apparent rate of heat release (RoHR) for PRF89 and PRF97 at stoichiometric*  
 283 *conditions.*

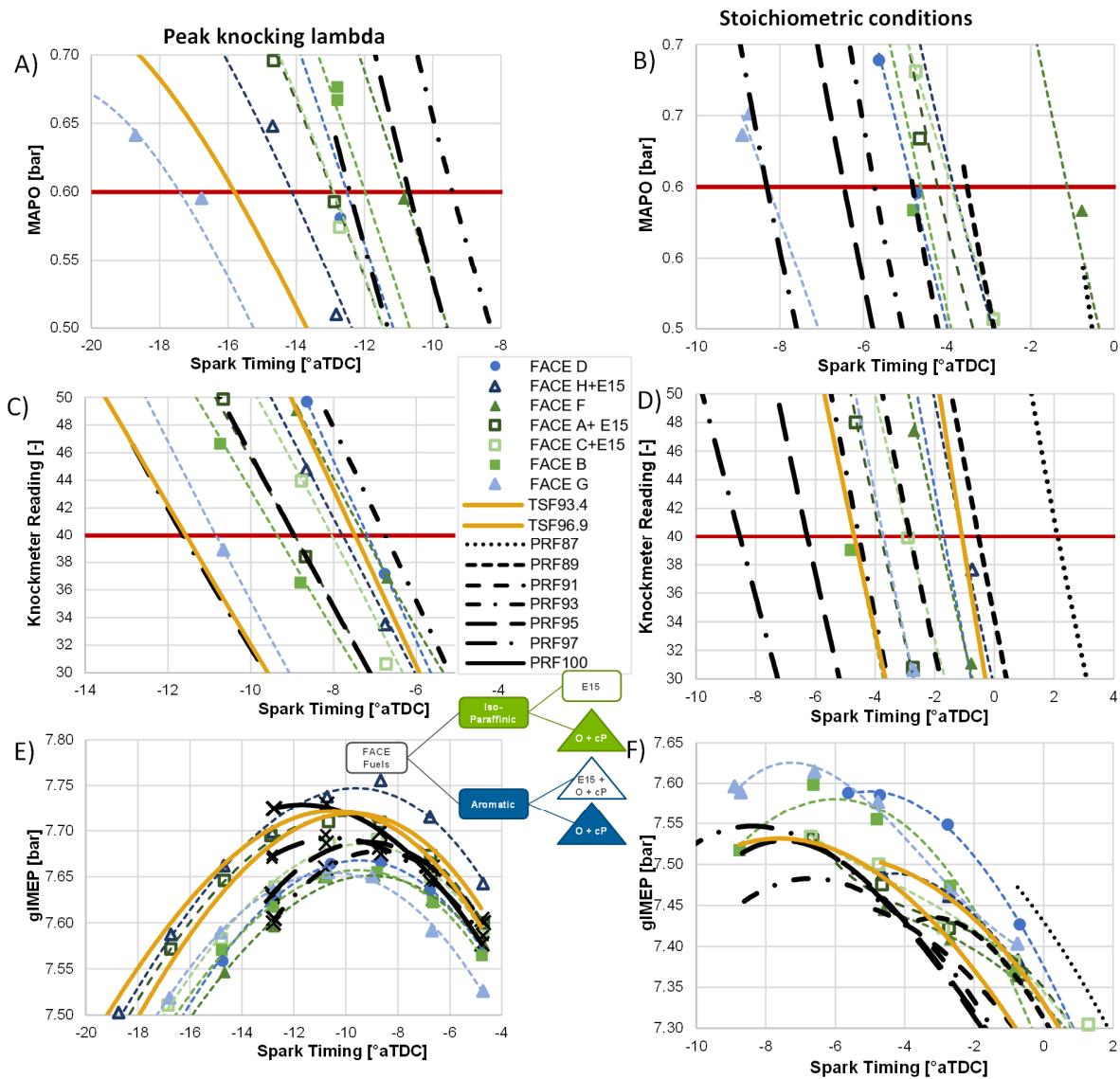
284 *Figure 5B shows a zoomed-in perspective of the green highlighted box from Figure 5A. The cylinder*  
 285 *pressures for PRF97 and PRF89 closely match up to -15°aTDC but diverge before spark timing. An analysis*  
 286 *of the apparent rate of heat release revealed a pre-spark heat release, also called low-temperature heat*  
 287 *release (LTHR). Multiple publications recently analyzed LTHR during compression-ignition as well as*  
 288 *spark-ignition modes [13, 21, 26, 27]. Generally, PRFs are prone to exhibit low-temperature chemistry*  
 289 *compared to toluene or ethanol blends. Also, LTHR was noticeable in spark-ignition operation when*  
 290 *retarding the spark timing [26]. The low-temperature heat release before spark timing caused an*  
 291 *increased cylinder pressure for PRF89. The higher RON PRF97 did not exhibit a noticeable LTHR.*  
 292 *Therefore,* the  
 293 *low-temperature chemistry for PRF89 increased the flame propagation and subsequently advanced the*  
 294 *center of combustion. For further analysis, the spark timing will be used as it was the varied parameter*  
 295 *during the experimental study and is not affected by increased flame propagation or low-temperature*  
 296 *heat release like CA50 would be.*

297

298

## 299 3.2. FACE Fuels

300 Spark timing sweeps similar to *Figure 3* were performed for all fuels mentioned in *Section 2*.  
301 *Experimental Procedure.* *Figure 6* shows the cylinder pressure-based knock intensity MAPO, the  
302 knockmeter knock intensity, and the gIMEP as a function of spark timing for the FACE fuels and the two  
303 TSFs in comparison to the previously discussed PRFs. While wide spark timing sweeps were performed,  
304 *Figure 6* focuses on the relevant spark timings at which either of the two knock thresholds or the  
305 maximum brake torque (MBT) was achieved. The tests were performed at peak knocking lambda (*Figure*  
306 *6A, C, E*), as well as at stoichiometric conditions (*Figure 6B, D, F*), which resembles modern engine  
307 operation. During experimental testing, both the knockmeter and MAPO knock intensity vary (compare  
308 [4]). Therefore, it is not possible to have an experimental data point directly at the knock threshold.  
309 Instead, for each fuel, a third-order regression polynomial was created for the MAPO and knockmeter  
310 response over a wide range of spark timings. An excellent curve fit was ensured with each coefficient of  
311 determination  $(R^2)$   
312 exceeding 0.99.



313

314 *Figure 6. Spark timing sweeps at peak knock lambda conditions (A, C, E) and stoichiometric conditions (B, D, F) for MAPO knock*

315 *intensity, knockmeter knock intensity, and gIMEP for all fuels.*

316 Fuel composition-specific differences in the MAPO-based KLSA can be seen in *Figure 6A* and *Figure 6B*.

317 Primarily paraffinic FACE fuels (green) tend towards a more retarded KLSA compared to aromatic

318 gasolines (blue) and highly aromatic TSFs (orange). At peak knocking lambda conditions, PRF97 had a

319 significantly retarded MAPO-based KLSA compared to highly aromatic fuels while it successfully

320 bracketed all fuels at stoichiometric conditions. *Figure 6C* and *Figure 6D* show the knockmeter-based

321 spark timing sweeps at which the PRFs bracketed all sample fuels. A composition-based (aromatic vs.  
322 paraffinic) trend was not apparent. At peak knocking lambda conditions, each spark timing sweep was  
323 performed past the maximum brake torque (MBT) timing while under stoichiometric conditions, PRF87  
324 did not reach the MBT timing. All MAPO and knockmeter-based KLSA as well as the MBT for  
325 stoichiometric conditions and PKL conditions are summarized in *Table 3*.

326 As can be seen from *Figure 6* and *Table 3*, the KSLA and MBT timing occur at a more advanced timing for  
327 PKL conditions compared to stoichiometric conditions. As shown in [4], the lambda of peak knock  
328 intensity is typically rich. When shifting to a stoichiometric condition, the knock intensity reduced when  
329 tested at a constant compression ratio. Under stoichiometric operation during this study, a higher  
330 compression ratio was used compared to PKL conditions which resulted in a more retarded combustion  
331 limitation under stoichiometric conditions. Under PKL conditions, the MBT timing occurred later than  
332 either KLSA timing. Therefore, the engine was not knock limited at the maximum torque output. For  
333 stoichiometric conditions, the operation at an increased compression ratio resulted in MBT timings  
334 earlier than KLSA timings. Additional spark advance beyond the knock threshold would benefit the  
335 combustion and result in increased torque output. For both PKL and stoichiometric operation, the crank  
336 angle difference between MAPO-based and knockmeter-based KLSA varied among the FACE fuels.  
337 Primary paraffinic FACE gasolines (FACE B, F, A+E15, and C+E15) show only small differences up to one  
338 crank angle degree while primary aromatic FACE gasolines typically show about two to four crank angle  
339 degrees later KLSA when based on the knockmeter. The PRFs did not always mirror this trend as it  
340 seemed dependent on the respective RON level of the PRF. The timing differences between knockmeter  
341 and MAPO-based KLSA for paraffinic and aromatic FACE fuels is due to the difference in knock intensity  
342 measurement characteristic. The MAPO is only considering pressure oscillations while the knockmeter is  
343 affected by the pressure rise rate as well [8]. Therefore, at a given MAPO knock intensity, the pressure  
344 rise rate of a chemical group of fuels can vary as shown in *Figure 7*.

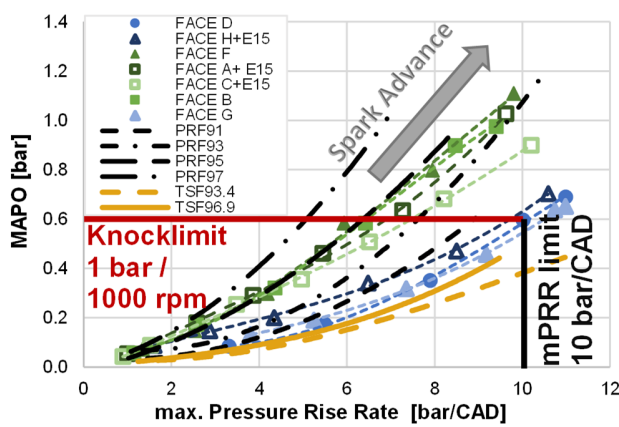
345 Table 3. Overview of KLSA data for PKL and stoichiometric operation based on MAPO and knockmeter knock intensity.

346 Legend: \* extrapolated | \*\* MBT not reached due to knock limitation of the engine | \*\*\* Knock threshold not reached

Fuel	Peak Knocking Lambda			Stoichiometric Conditions		
	MAPO KLSA [°aTDC]	Knockmeter KLSA [°aTDC]	Location of MBT [°aTDC]	MAPO KLSA [°aTDC]	Knockmeter KLSA [°aTDC]	Location of MBT [°aTDC]
FACE-B	-12.0	-13.3	-8.8	-4.6	-4.7	-6.6
FACE-D	-12.5	-10.2	-8.6	-4.8	-1.7	-5.2
FACE-F	-10.8	-10.7	-8.9	-1.1	-1.8	-4.6
FACE-G	-17.4	-14.3	-10.7	-8.3	-3.7	-6.6
FACE-A + E15	-12.9	-12.9	-10.7	-4.2	-3.8	-6.7
FACE-C + E15	-12.9	-11.8	-8.8	-3.9	-2.9	-6.7
FACE-H + E15	-14.1	-11.3	-8.7	-3.8	-1.1	-4.6
PRF87	Not tested	Not tested	Not tested	-1.0	+2.1	N/A**
PRF89	Not tested	Not tested	Not tested	-3.5	-0.5	N/A**
PRF91	Not tested	Not tested	Not tested	-4.8	-2.8	N/A**
PRF93	-9.8	-10.0	-8.7	-5.7	-4.5	-5.7
PRF95	-10.8	-12.4	-10.7	-6.5	-6.3	-8.7
PRF97	-12.4	-15.4	-10.7	-8.3	-8.5	-8.7
PRF100	-17.3 *	-18.5	-10.7	Not tested	Not tested	Not tested
TSF93.4	-15.8	-10.6	-10.7	-6.4	-1.1	N/A**
TSF96.9	N/A***	-15.5	-10.7	-10.3	-4.7	-8.8

347

348 As previously mentioned, the pressure-based knock intensity threshold was selected to 0.6 bar,  
 349 representing 1 bar cylinder pressure oscillations per 1000 rpm. For stoichiometric operation, *Figure 7*  
 350 correlates the 300 cycle-averaged MAPO and the maximum pressure rise rate for the spark timing  
 351 sweeps of the FACE fuels, PRFs, and TSFs. Advanced spark timing led to both a higher MAPO knock  
 352 intensity as well as maximum pressure rise rate. A clear distinction between mainly paraffinic (green)  
 353 and primarily aromatic (blue) fuels can be observed. Highly paraffinic fuels showed a much reduced  
 354 maximum pressure rise rate which supports the previously discussed smaller crank angle degree  
 355 difference between knockmeter- and MAPO-based KLSA for *Figure 6* and *Table 3*. Similarly, the PRFs and  
 356 TSFs support the clear distinction between primarily paraffinic and aromatic fuels based on their  
 357 difference in maximum pressure rise rate at a given MAPO knock intensity.



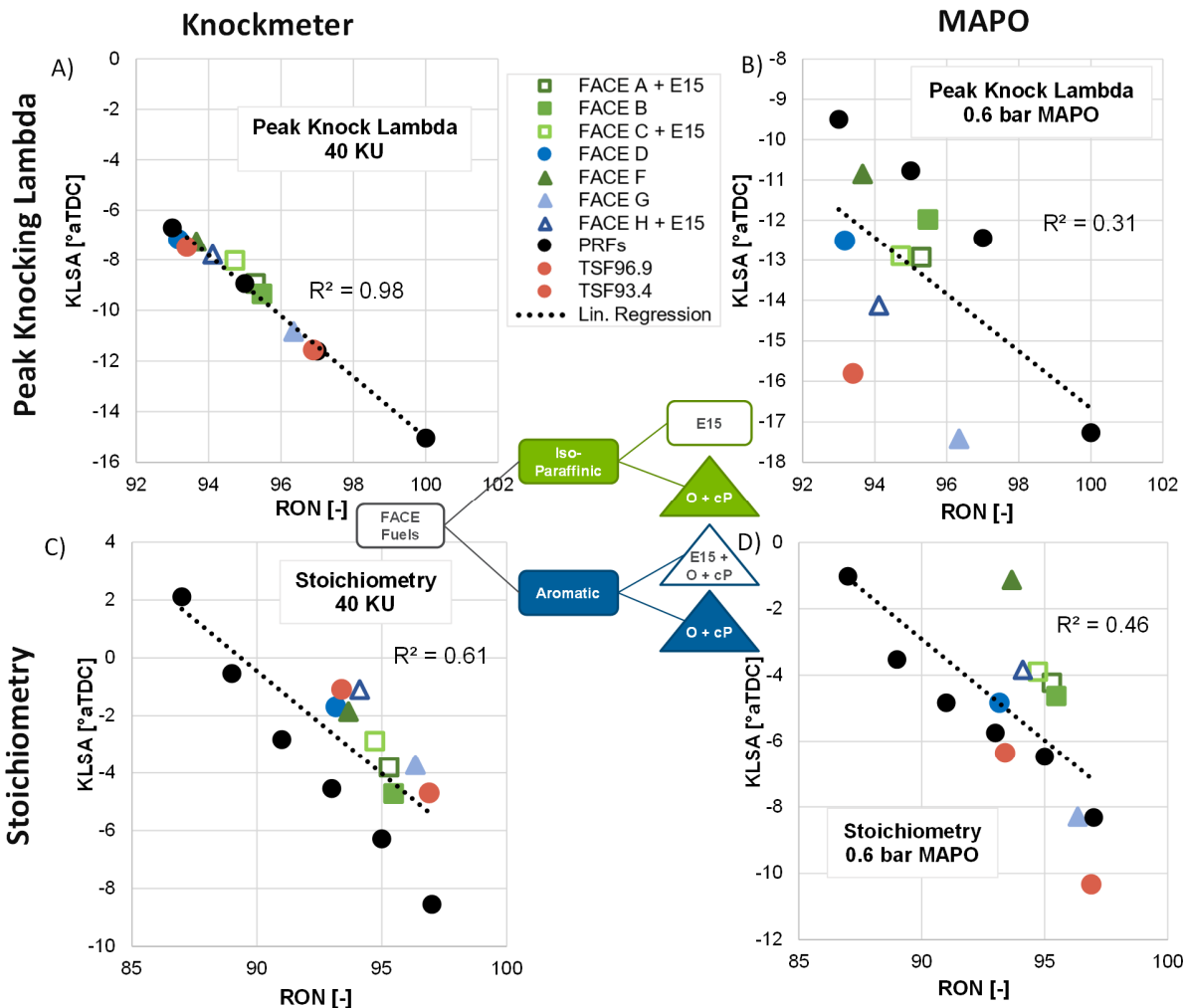
358  
 359 *Figure 7. Correlation between the maximum amplitude of pressure oscillations (MAPO) and the maximum pressure rise rate*  
 360 *(mPRR) at stoichiometric conditions with defined operation thresholds.*  
 361 For further analysis, only the MAPO knock intensity limit was applied and the maximum pressure rise  
 362 rate limit was neglected to ensure all fuels would be rated based on a common characteristic. It was also  
 363 found that a reduced MAPO threshold resulted in an identical order of fuels while not reaching the  
 364 maximum pressure rise rate threshold.

365

366    **4. KLSA-based Octane Correlations**

367

368    Knock assessment in modern engines as characterized by the knock limited spark advance (KLSA) based  
369    on a pressure-based knock intensity threshold is widely common but its correlation to the standard RON  
370    rating of the fuel is often inadequate [5, 6, 13, 20]. *Figure 8* shows the KLSA of FACE fuels, PRFs, and TSFs  
371    under PKL (*Figure 8A* and *Figure 8B*) and stoichiometric (*Figure 8C* and *Figure 8D*) conditions compared  
372    to the standard RON rating of the fuels. The previous publication showed significant differences in the  
373    knock intensity response for lambda sweeps which will impact the KLSA ratings between the two  
374    conditions [4]. For both PKL and stoichiometric operation, the knock threshold was based on either 0.6  
375    bar maximum amplitude of pressure oscillations (*Figure 8B, D*) or a knockmeter reading of 40 KU (*Figure*  
376    *8A, C*). For each plot within *Figure 8*, a linear trendline for all fuels along with its coefficient of  
377    determination ( $R^2$ ) is shown to quantitatively evaluate the correlation. Across all plots, increased RON  
378    generally allowed for more spark advance but important discrepancies between fuels were observed.



379

380 *Figure 8. Correlations between the knock limited spark advance (KLSA) and standard RON ratings for varying operating*  
 381 *conditions.*

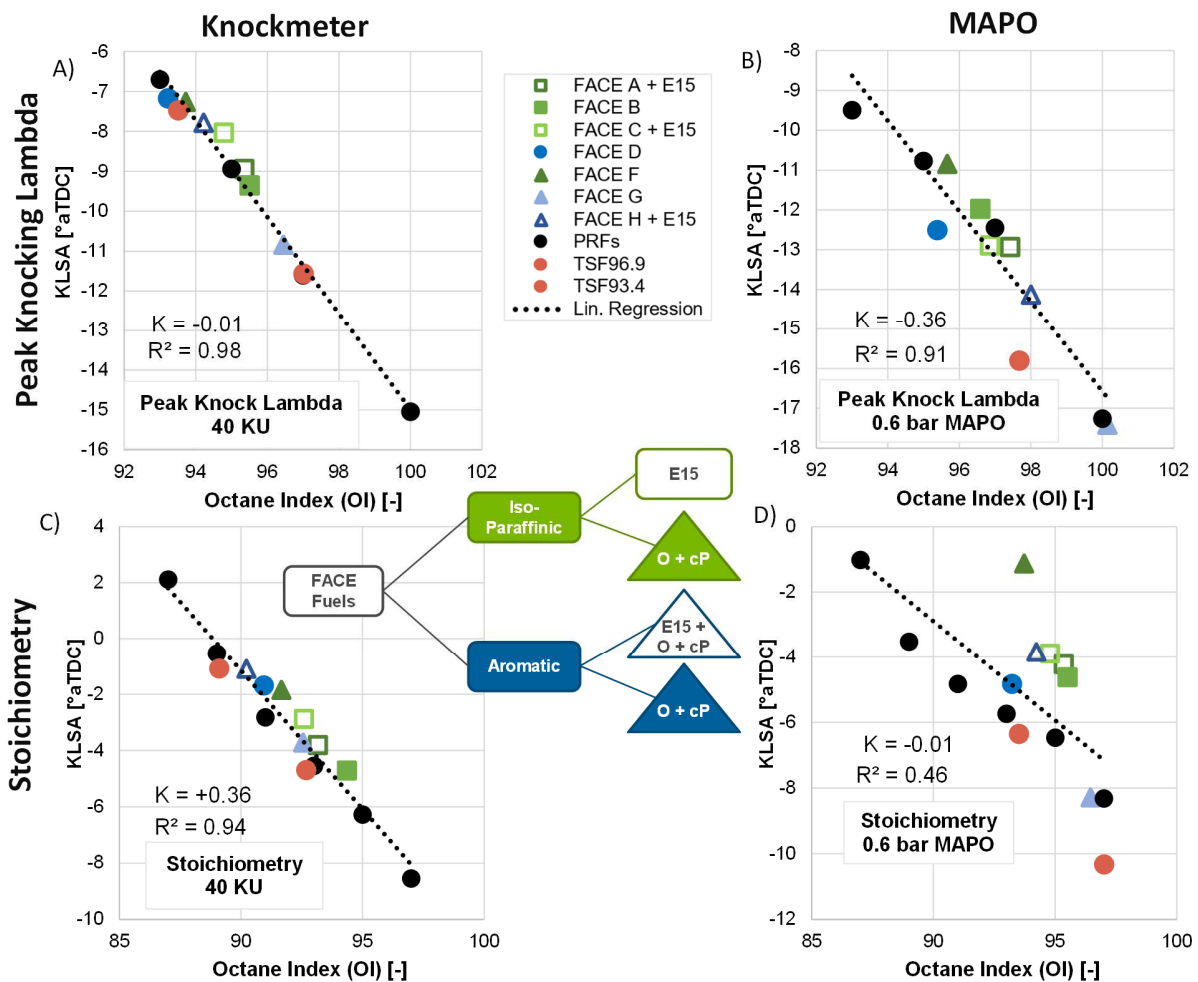
382 An excellent correlation was found between the knockmeter-based KLSA at PKL operation and RON,  
 383 *Figure 8A.* This can be explained by the similarity between the testing conditions and the standard RON  
 384 test which both use the same air-to-fuel ratio as well as knock intensity characterization method. Only  
 385 the spark timing and hence the knock intensity differ. Generally, the KLSA showed better correlations  
 386 when based on the knockmeter compared to MAPO. When keeping PKL operation but using a MAPO  
 387 threshold, the correlation significantly reduced to  $R^2 = 0.3$ , *Figure 8B.* This poor correlation followed  
 388 previous findings of the first publication, where the MAPO knock intensity during a standard RON rating

389 did not correlate to the fuel's RON rating [4]. As a result, the KLSA for the fuels also varies significantly.  
390 The PRFs previously showed the highest MAPO ratings and hence required the most retarded spark  
391 timings at PKL conditions. Furthermore, primarily paraffinic FACE fuels (green markers) showed the  
392 second most retarded KLSAs which aligns with the slightly reduced MAPO ratings compared to PRFs in  
393 the first publication [4]. Predominantly aromatic FACE fuels (blue markers) and mostly aromatic TSFs  
394 (orange markers) tended towards the most advanced KLSAs following their previously described lower  
395 MAPO ratings under standard RON conditions.

396 When shifting operation from PKL (*Figure 8A*) to stoichiometric (*Figure 8C*), the correlation between  
397 knockmeter and RON reduced significantly due to the larger deviation from the standard RON test. The  
398 PRFs showed the most advanced KLSA while all falling on a separate imaginary trendline. The advanced  
399 KLSA of PRFs in *Figure 8C* is contradicting the most retarded KLSA of PRFs in *Figure 8B*. This can be  
400 explained by the different methods of evaluating knock intensity. Among a common knockmeter  
401 reading, the MAPO reading changes significantly with fuel composition. Furthermore, as shown in the  
402 previous study, the lambda dependence of knock intensity needs consideration as the lambda of peak  
403 knock intensity for PRFs was the richest at approximately  $\lambda = 0.88 - 0.89$  [4]. Subsequently, the PRFs  
404 underwent the largest lambda change when switching from PKL to stoichiometric which resulted in the  
405 largest effect on knock intensity. This hypothesis was confirmed by FACE-B, which had the second  
406 richest PKL in the previous study and now showed a slightly advanced KLSA amongst the FACE fuels in  
407 *Figure 8C* [4]. Furthermore, FACE-H+E15 and FACE-G show the most retarded KLSA in *Figure 8C* while  
408 having the closest to stoichiometric peak knocking lambda in the previous study [4]. For stoichiometric  
409 operation, the MAPO-based KLSA correlation to RON in *Figure 8D* is poor but slightly improved upon  
410 MAPO-based PKL operation in *Figure 8B*. The authors previously showed that a MAPO-based RON at  
411 stoichiometric conditions somewhat correlated to the standard RON ratings amongst the FACE fuels [4].  
412 *Figure 8D* shows the FACE fuels grouped by their chemical composition. In contrast, the PRFs fall on a

413 separate imaginary trendline which reduced the overall correlation. Of the FACE fuels, the mainly  
414 paraffinic blends (green markers) showed a more retarded KLSA compared to the aromatic fuels (blue  
415 markers). This was in line with findings from the previous study by the authors which showed that the  
416 effective MAPO-based RON at stoichiometric conditions for aromatic fuels was close to the standard  
417 RON rating while that of primarily paraffinic FACE fuels had a lower effective MAPO-based RON at  
418 stoichiometric conditions than their standard RON rating [4]. This translates to the KLSA grouping of  
419 aromatic and paraffinic FACE fuels in *Figure 8D*. It is also noted that the TSFs showed the most advanced  
420 KLSA while having the highest concentration of aromatic components.

421 *Figure 8* compared the KLSAs for all fuels to their standard RON with correlations ranging from very  
422 good ( $R^2 = 0.98$ ) in the case of a knockmeter-based PKL operation to poor ( $R^2 = 0.31$ ) for MAPO-based  
423 PKL operation. Literature shows Octane Index to better correlate to modern engine operation which  
424 includes the use of a cylinder pressure-based knock intensity like MAPO. *Figure 9* shows the identical  
425 KLSA data from *Figure 8* but compares it to Octane Index, which was calculated using equation 1 and the  
426 standard RON and MON values of the fuels. Each correlation was optimized for the highest coefficient of  
427 determination ( $R^2$ ) by altering the engine operation-specific K-factor. Both coefficients are shown on  
428 each plot in *Figure 9*.



429

430 *Figure 9. Correlations between the knock limited spark advance (KLSA) and Octane Index for varying operating conditions with*  
 431 *K optimized for the best correlation.*

432 The KLSA for the knockmeter threshold under PKL operation already strongly correlated to the RON  
 433 ratings of the fuels in *Figure 8*. This was no surprise and was due to the similarity to the standard RON  
 434 test as it only deviated in terms of knock threshold and spark timing. The introduction of Octane Index  
 435 did not further improve the coefficient of determination and the engine operation-specific factor K is  
 436 essentially zero, *Figure 9A*. Switching to a MAPO-based knock threshold at PKL conditions, KLSA showed  
 437 the worst correlation to RON in *Figure 8B*. This is in line with findings from the first part of this three-  
 438 part publication series where MAPO under standard RON conditions did not correlate to the fuel's

439 standard RON rating [4]. The first part showed mainly paraffinic fuels with increased MAPO knock  
440 intensities under standard RON conditions compared to aromatic fuels which resulted in a more  
441 retarded KSLA in *Figure 8* [4]. Switching to Octane Index significantly improved the correlation to KLSA  
442 but required a K-factor of  
443  $K = -0.36$ , *Figure 9B*. This again is very similar to the findings from the first part which showed the best  
444 correlation between MAPO and Octane Index at  $K = -0.48$  [4]. A negative K-factor effectively means  
445 engine operation at beyond RON conditions while the engine mostly operates under RON conditions  
446 except for the knock threshold and spark timing. Knock limited spark advance studies in the literature  
447 typically associate  $K = 0$  with RON conditions but this study suggests a slightly negative K-factor would  
448 yield a better comparison when using a MAPO-based knock threshold. Moving towards stoichiometric  
449 conditions and using a knockmeter-based threshold, the KLSA correlation to Octane Index greatly  
450 improved compared to standard RON, *Figure 8C* and *Figure 9C*. While the knockmeter was largely  
451 affected by the gap between PKL and stoichiometric, Octane Index counteracted that effect and yielded  
452 an excellent correlation. It is noted that the  $K = +0.36$  showed a distinct move towards the fuel's  
453 antiknock index ( $K = 0.5$ ). Furthermore, the combined findings from *Figure 8C* and *Figure 9C* suggest that  
454 the lambda of peak knock and the RON-MON sensitivity could be linked since the RON-MON sensitivity  
455 and the PKL mostly moved coherently. While MON testing is not part of this three-part series, it is noted  
456 that literature shows a generally closer to stoichiometric PKL under MON conditions [28]. When  
457 operating the engine with a MAPO-based threshold at stoichiometric conditions, which best resembles  
458 modern engine testing, no benefit of Octane Index over RON was found and the coefficient of  
459 determination remained low with a K-factor of around zero, *Figure 8C* and *Figure 9D*. This disappointing  
460 correlation with some recognizable trend with RON and Octane Index is in line with literature which  
461 shows an improvable correlation between RON and KLSA data tested on modern SI research engines [8,  
462 13, 20]. It is also noted that varying the knock threshold outside of 0.6 bar MAPO or 40 knockunits

463 affected the KLSA accordingly but the correlations from *Figure 8* and *Figure 9*, as well as the K-factor  
464 optimizations, remained largely similar.

465 The standard octane test rates the knock intensity of a sample fuel relative to that of PRFs. Applying a  
466 similar methodology, the measured KLSA values of the sample fuels are normalized by the KLSAs of  
467 respective PRFs. Subsequently, an effective octane number based on KLSA was calculated using  
468 interpolation between the applicable PRFs. *Table 4* shows the effective octane numbers for the  
469 knockmeter- and MAPO-based KLSA values on the basis of KLSA values from *Table 3*. For comparison,  
470 *Table 4* also shows the standard RON of each fuel. The calculations were performed for stoichiometric  
471 conditions as well as each fuel under its individual peak knocking lambda operation. While most KLSA-  
472 based effective RONs were interpolated, some fuels had their KLSA value outside of the boundaries set  
473 by the PRFs and required extrapolation. The correlation between the calculated effective KLSA-based  
474 RONs to the standard RON would follow the trends shown in and described for *Figure 8*.

475 The additional value of the effective RON calculations is the order of sample fuels relative to PRFs. For  
476 FACE fuels and TSFs, the effective knockmeter KLSA-based RON at PKL is within 0.8 octane of their  
477 standard RON with is only slightly outside the 0.7 RON reproducibility of the standard RON test. Using a  
478 MAPO-based knock intensity evaluation under PKL conditions, the effective RON of the FACE fuels and  
479 TSFs increased in comparison to their standard RON suggesting that they had a retarded KLSA compared  
480 to PRFs. On the contrary, the MAPO-based RON under stoichiometry significantly reduced the effective  
481 RON compared to both standard RON and PKL MAPO RON for most of the sample fuels with the  
482 exception of FACE-G and both TSFs. These are the fuels with the highest RON-MON sensitivity as well as  
483 the highest aromatic content.

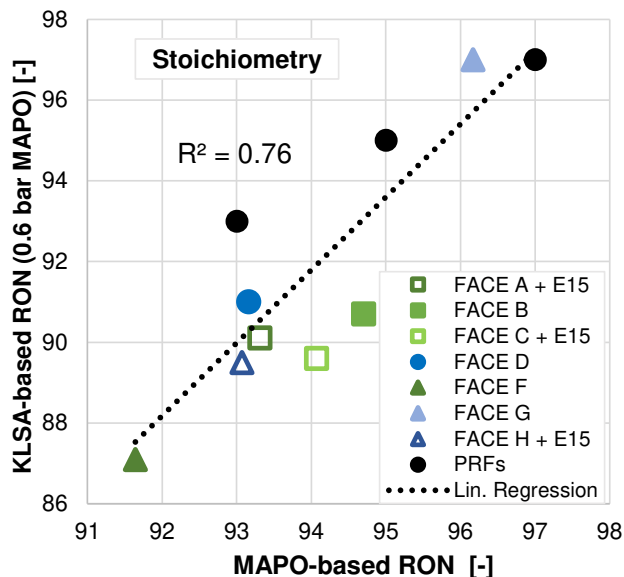
484

485 Table 4. Overview of KLSA-based RON values for PKL and stoichiometric operation based on MAPO (0.6 bar) and knockmeter  
 486 (40 KU) knock intensity.  
 487 Legend: \* extrapolated | \*\* RON defined based on volumetric iso-octane content | \*\*\* did not reach the knock threshold

Fuel	Standard RON	Peak Knocking Lambda		Stoichiometric	
		MAPO KLSA-based RON [-]	Knockmeter KLSA-based RON [-]	MAPO KLSA-based RON [-]	Knockmeter KLSA-based RON [-]
FACE-B	95.8	96.4	95.3	90.7	93.2
FACE-D	94.2	97.1	93.4	91.0	90.0
FACE-F	94.0	95.1	93.5	87.1	90.1
FACE-G	96.5	100.1*	96.4	97.0	92.0
FACE-A + E15	94.8	97.6	95.0	90.1	92.1
FACE-C + E15	94.8	97.5	94.2	89.6	91.1
FACE-H + E15	94.1	98.0	94.0	89.5	89.5
PRF87**	87	Not tested	Not tested	87	87
PRF89**	89	Not tested	Not tested	89	89
PRF91**	91	Not tested	Not tested	91	91
PRF93**	93	93	93	93	93
PRF95**	95	95	95	95	95
PRF97**	97	97	97	97	97
PRF100**	100	100	100	Not tested	Not tested
TSF93.4	93.4	99.1	93.7	94.7	89.5
TSF96.9	96.9	N/A***	97.0	99.2*	93.2

488

489 The KLSA-based effective RON ratings from *Table 4* under stoichiometric operation using a MAPO knock  
490 intensity threshold best represent how modern commercial engines perform knock testing but *Figure 8*  
491 showed a poor correlation to its standard RON while switching to Octane Index in *Figure 9* also did not  
492 improve upon it. *Figure 10* shows a comparison of the effective KLSA-based RON rating from this study  
493 to the MAPO-based effective RON from the previous work [4]. Both tests were conducted using a  
494 MAPObased knock intensity under stoichiometric conditions. Only fuels that were common between  
495 both test sets are displayed. The PRFs have a defined effective RON rating based on their volumetric  
496 concentration of iso-octane. Subsequently, they are expected to exactly line up. The overall correlation  
497 as quantitively expressed by the coefficient of determination is acceptable. Except for FACE-G, all FACE  
498 fuels showed a higher MAPO-based RON. The difference between the two datasets is in the spark timing  
499 and the level of knock intensity. Most of the FACE fuels showed a slight reduction in relative knock  
500 resistance when tested under KLSA conditions which could result from the retarded spark timing or the  
501 reduced level of knock intensity or a combined effect of both parameters. Subsequently, the third study  
502 of this publication series will combine these findings and maintain constant combustion phasing as well  
503 as a constant knock intensity by varying the compression ratio.



504

505 *Figure 10. Comparison of the KLSA-based effective RON results with the MAPO-based effective RON from the previous work [4].*

506

507 **5. Summary**

508

509 The observations of this work can be summarized as follows:

510 - Knock-limited spark advance sweeps were performed for FACE and reference fuels on the  
 511 standard octane rating CFR engine under peak knocking lambda and stoichiometric operation  
 512 for a knockmeter- and a maximum amplitude of pressure oscillation-based (MAPO) knock  
 513 intensity threshold.

514 - The use of knock-limited spark advance (KLSA) proved superior compared to the knock-limited  
 515 combustion phasing (KLCA50). A detailed heat release analysis found autoignition to occur  
 516 simultaneously to the center of combustion which caused undesirable effects on KLCA50. Low-  
 517 temperature heat release before spark timing occurred for low RON PRFs at retarded spark  
 518 timings.

519 - Primarily paraffinic fuels tended towards higher pressure oscillations while fuels with increased  
520 aromatic content showed higher pressure rise rates.

521 - A knockmeter-based KLSA under PKL conditions showed the best correlation to RON due to its  
522 similarity to the standard RON test. Using a MAPO-based knock intensity threshold under PKL  
523 conditions resulted in a poor correlation to RON. Shifting from RON to Octane Index significantly  
524 improved the correlation to an excellent fit but at a K-factor of  $K = -0.36$  which resembles RON-  
525 like KLSA testing on modern engine platforms. A MAPO-based stoichiometric KLSA similar to  
526 modern engine knock testing had a poor correlation to RON while Octane Index only slightly  
527 improved the correlation which validates the limited applicability of RON in modern engine  
528 operation.

529 - The KLSA-based stoichiometric RON using a MAPO knock intensity threshold correlated  
530 reasonably well with the MAPO-based stoichiometric RON from the first part of this publication  
531 series. All but FACE-G showed an offset towards increased MAPO-based RON.

532

533 This study applied the methods of modern engine knock characterization to the standard octane rating  
534 CFR engine. A MAPO-based KLSA rating under stoichiometry showed only a poor correlation to RON or  
535 Octane Index. A better correlation was found between the KLSA-based stoichiometric RON and the  
536 MAPO-based stoichiometric RON from the first study of this three-part publication series. However,  
537 except for FACE-G, all FACE fuels showed slightly increased MAPO-based RON results. Since both the  
538 knock intensity and the spark timing varied simultaneously, a final answer to the cause of this offset is  
539 targeted for the third study. The interlinked parameters combustion phasing and knock intensity will be  
540 kept constant by varying the compression ratio.

541

542

543 **6. Acknowledgments**

544

545 The authors would like to thank the Coordinating Research Council (CRC) task group Advanced Vehicle  
546 Fuel Lubricants AVFL-32 for providing the FACE fuels, funding, and project guidance.

547 The authors would also like to acknowledge the support and contribution of Dr. Scott Miers, thank  
548 Stephan Schneider for his assistance during the experimental work, and thank Timothy Rutter for his  
549 technical support.

550 Argonne is a U.S. Department of Energy laboratory managed by UChicago Argonne, LLC under contract  
551 DE-AC02-06CH11357.

552

553 **7. References**

554

- 555 1. Swarts, A. and Yates, A., "Insights into the Role of Autoignition during Octane Rating," SAE  
556 Technical Paper 2007-01-0008, 2007, doi.org/10.4271/2007-01-0008.
- 557 2. ASTM D2699-15a, "Standard Test Method for Research Octane Number of Spark-Ignition Engine  
558 Fuel," ASTM International, West Conshohocken, PA, 2015, doi: 10.1520/D2699-15A
- 559 3. ASTM D2700-16, " Standard Test Method for Motor Octane Number of Spark-Ignition Engine  
560 Fuel," ASTM International, West Conshohocken, PA, 2016, doi: 10.1520/D2400-16
- 561 4. Hoth, A., Kolodziej, C., "Effects of knock intensity measurement technique and fuel chemical  
562 composition on the research octane number (RON) of FACE gasolines: Part 1 – Lambda and

563 knock characterization", Fuel, Volume 304, 2021, 120722,ISSN 0016-2361,  
564 <https://doi.org/10.1016/j.fuel.2021.120722>.

565 5. Swarts, A., Yates, A., Viljoen, C., and Coetzer, R., "A Further Study of Inconsistencies between  
566 Autoignition and Knock Intensity in the CFR Octane Rating Engine," SAE Technical Paper 2005-  
567 01-2081, 2005, doi:10.4271/2005-01-2081.

568 6. Swarts, A., Anderson, G., and Wallace, J., "Comparing Knock between the CFR Engine and a  
569 Single Cylinder Research Engine," SAE Technical Paper 2019-01-2156, 2019.

570 7. Huber, K., Hauber, J., Raba, A., and Nell, R., "New Test Procedure to Determine Fuel's Knock  
571 Resistance," MTZ-Motortechnische Zeitschrift 74(7/8):62-69, 2013.

572 8. Rockstroh, T., Kolodziej, C., Jespersen, M., et al., "Insights into Engine Knock: Comparison of  
573 Knock Metrics across Ranges of Intake Temperature and Pressure in the CFR Engine," SAE  
574 Technical Paper 2018-01-0210, 2018, doi:10.4271/2018-01-0210.

575 9. Heywood, J., "Internal Combustion Engine Fundamentals," New York: McGraw-Hill, 1998. ISBN:  
576 0-07-028637-X

577 10. Hoth, A., Kolodziej, C., Rockstroh, T. et al., "Combustion Characteristics of Match-Blended PRF  
578 and TSF Fuels with Ethanol in an Instrumented CFR Engine," SAE Technical Paper 2018-01-1672.

579 11. Hauber, J., Huber, K., and Nell, R., "New GKI - Gasoline Knock Index for Rating of Fuel's Knock  
580 Resistance on an Upgraded CFR Test Engine," SAE Technical Paper 2018-01-1743, 2018.

581 12. Hoth, A., Pulpeiro Gonzalez, J., Kolodziej, C., and Rockstroh, T., "Effects of Lambda on Knocking  
582 Characteristics and RON Rating," SAE Int. J. Adv. & Curr. Prac. in Mobility 1(3):1188-1201,  
583 2019, <https://doi.org/10.4271/2019-01-0627>.

584 13. J. Szybist, D. Splitter, "Understanding chemistry-specific fuel differences at a constant RON in a  
585 boosted SI engine", Fuel, Volume 217, 2018, Pages 370-381, doi:10.1016/j.fuel.2017.12.100.

586 14. Yates, A., Swarts, A., and Viljoen, C., "Correlating Auto-Ignition Delays And Knock-Limited Spark-  
587 Advance Data For Different Types Of Fuel," SAE Technical Paper 2005-01-2083,  
588 2005, doi:10.4271/2005-01-2083.

589 15. Kalghatgi, G., "Fuel Anti-Knock Quality - Part I. Engine Studies," SAE Technical Paper 2001-01-  
590 3584, 2001, doi:10.4271/2001-01-3584.

591 16. Morgan, N., Smallbone, A., Bhave, A., et al., "Mapping surrogate gasoline compositions into  
592 RON/MON space", Combustion and Flame, Volume 157, Issue 6, 2010, Pages 1122-1131,  
593 <https://doi.org/10.1016/j.combustflame.2010.02.003>.

594 17. Mittal, V. and Heywood, J., "The Shift in Relevance of Fuel RON and MON to Knock Onset in  
595 Modern SI Engines Over the Last 70 Years," SAE Int. J. Engines 2(2):1-10, 2010,  
596 doi:10.4271/2009-01-2622.

597 18. Kolodziej, C., Pamminger, M., Sevik, J., Wallner, T. et al., "Effects of Fuel Laminar Flame Speed  
598 Compared to Engine Tumble Ratio, Ignition Energy, and Injection Strategy on Lean and EGR  
599 Dilute Spark Ignition Combustion," SAE Int. J. Fuels Lubr. 10(1):82-94,  
600 2017, <https://doi.org/10.4271/2017-01-0671>.

601 19. Pulpeiro Gonzalez, J., Shah, A., Hoth, A., Rockstroh, T. et al., "Statistical Analysis of Fuel Effects  
602 on Cylinder Conditions Leading to End-Gas Autoignition in SI Engines," SAE Technical Paper  
603 2019-01-0630, 2019, <https://doi.org/10.4271/2019-01-0630>.

604 20. Vuilleumier, D., Kim, N., Sjöberg, M., Yokoo, N. et al., "Effects of EGR Constituents and Fuel  
605 Composition on DISI Engine Knock: An Experimental and Modeling Study," SAE Technical Paper  
606 2018-01-1677, 2018, doi:10.4271/2018-01-1677.

607 21. Waqas, M., Hoth, A., Kolodziej, C., Rockstroh, T. et al., "Characterization of Low Temperature  
608 Reactions in the Standard Cooperative Fuel Research (CFR) Engine," *SAE Int. J. Engines* 12(5):597-  
609 610, 2019, <https://doi.org/10.4271/03-12-05-0038>.

610 22. Cannella, W., Foster, M., Gunter, G., et al., "FACE Gasolines and Blends with Ethanol: Detailed  
611 Characterization of Physical and Chemical Properties", CRC Report No. AVFL-24, 2014.

612 23. Pulpeiro Gonzalez, J., Hall, C., Kolodziej, C., "Determination of a most representative cycle from  
613 cylinder pressure ensembles via statistical method using distribution skewness", International  
614 Journal of Engine Research, 2021. <https://doi.org/10.1177/14680874211065525>.

615 24. Lavoie, G., Ortiz-Soto, E., Babajimopoulos, A., et al., "Thermodynamic sweet spot for high-  
616 efficiency, dilute, boosted gasoline engines", International Journal of Engine Research, Vol 14,  
617 Issue 3, 2013. <https://doi.org/10.1177%2F1468087412455372>

618 25. AVL Group, "Pressure Sensors For Combustion Analysis", Product Catalog, 01/2013.

619 26. Waqas, M., Hoth, A., Kolodziej, C., et al., "Detection of low temperature heat release (LTHR) in  
620 the standard Cooperative Fuel Research (CFR) engine in both SI and HCCI combustion modes",  
621 Fuel, Volume 256, 2019, <https://doi.org/10.1016/j.fuel.2019.115745>.

622 27. Waqas, M., Cheng, S., Goldsborough, S., et al., "An experimental and numerical investigation to  
623 characterize the low-temperature heat release in stoichiometric and lean combustion",  
624 Proceedings of the Combustion Institute, Volume 38, Issue 4, 2021, Pages 5673-5683,  
625 <https://doi.org/10.1016/j.proci.2020.07.146>.

626 28. Morganti, K., Foong, T., Brear, M., Da Silva, G. et al., "Design and Analysis of a Modified CFR  
627 Engine for the Octane Rating of Liquefied Petroleum Gases (LPG)," *SAE Int. J. Fuels Lubr.* 7(1):283-  
628 300, 2014, <https://doi.org/10.4271/2014-01-1474>.

629 **8. Abbreviations**

630

631 CA50 50% Mass Fraction Burned

632 CA90 90% Mass Fraction Burned

633 CFR Cooperative Fuel Research

634 CRC Coordinating Research Council

635 FACE Fuels for Advanced Combustion Engines

636 gIMEP Gross Indicated Mean Effective Pressure

637 KLCA50 Knock Limited Combustion Phasing

638 KLSA Knock Limited Spark Advance

639 KU Knock Units

640 MAPO Maximum Amplitude of Pressure Oscillations

641 MBT Maximum Brake Torque

642 MON Motor Octane Number

643 OI Octane Index

644 PRF Primary Reference Fuel

645 RON Research Octane Number

646 TSF Toluene Standardization Fuel

647

648 9. Appendix

649

650 *Table 5. Combustion research measurement and instrumentation systems employed on the Argonne CFR engine.*

<b>Crankshaft angle-based measurements</b>	
<b>Crank-angle based DAQ</b>	AVL IndiMicro & crankshaft encoder
<b>Spark timing</b>	Current clamp on coil wire
<b>Intake pressure</b>	Flush-mounted Kulite ETL-189-190M-2.5bara (0.2 crank-angle resolution)
<b>Exhaust pressure</b>	Flush-mounted Kulite EWCTV-312M-3.5bara (0.2 crank-angle resolution)
<b>Cylinder pressure</b>	AVL GU13Z-24 flush-mounted spark plug pressure transducer (0.1 crank angle resolution)
<b>Time-based measurements</b>	
<b>Time-based DAQ</b>	LabVIEW
<b>Intake pressure</b>	Setra 3550 pressure transducer
<b>Exhaust pressure</b>	Setra 3550 pressure transducer
<b>Intake, mixture, exhaust, coolant, and oil temperature</b>	K-type thermocouples
<b>Fuel rate</b>	Emerson CMF010M Coriolis Meter
<b>Lambda</b>	Bosch wide-band lambda sensor LSU 4.9
<b>CFR knock units</b>	Data-logged knockmeter signal

651

652